Contract No.:

This manuscript has been authored by Savannah River Nuclear Solutions (SRNS), LLC under Contract No. DE-AC09-08SR22470 with the U.S. Department of Energy (DOE) Office of Environmental Management (EM).

Disclaimer:

ARTICLE

Characterizing the solid hydrolysis product, $UF_4(H_2O)_{2.5}$, generated from neat water reactions with UF_4 at room temperature

Received 00th January 20xx,
Accepted 00th January 20xx

DOI: 10.1039/x0xx00000x

Jonathan H. Christian,[a] Christopher A. Klug,[b‡] Michael DeVore II,[a] Eliel Villa-Aleman,[a] Bryan J. Foley,[a] Nicholas Groden,[a] A. Taylor Baldwin,[a] Matthew S. Wellons*[a]

Uranium tetrafluoride (UF_4) is an important intermediate in the production of UF_6 and uranium metal. Room temperature hydrolysis of UF_4 was investigated using a combination of Fluorine-19 nuclear magnetic resonance spectroscopy (^{19}F NMR), Raman and infrared spectroscopy, powder X-ray diffraction, and microscopy measurement. $UF_4(H_2O)_{2.5}$ was identified as the primary solid hydrolysis product when anhydrous UF_4 was stirred in deionized water. Static NMR and ^{19}F magic angle spinning NMR measurements revealed that a small amount of uranyl fluoride can also form when anhydrous UF_4 is left in water, although this species comprises less than 5% of the total sample with the remaining parts being $UF_4(H_2O)_{2.5}$. Since UF_4 is generally considered to be stable under ambient conditions, these findings mark the first time that a room temperature reaction between UF_4 and water has been detected and analyzed without interference from additional chemical reagents. The Raman characterization of $UF_4(H_2O)_{2.5}$ presented herein is the first on record. Since UF_4 is one of the most used intermediates during chemical conversion of uranium ore to uranium metal for nuclear fuel and weapons, the results presented herein are applicable to numerous nuclear science fields where solid state detection of uranium is of value, including nuclear nonproliferation, nuclear forensics, and environmental remediation.

Introduction

Improved understanding of the reactivity and structural properties of nuclear materials remains a key goal in the fields of nuclear nonproliferation, nuclear forensics, radiochemistry, and environmental remediation.[1,2] Of particular importance, is the reactivity and chemical fate of solid state uranium materials as they interact with environmental factors, like ultraviolet radiation, water, and heat.[3,4,5] Water is perhaps the most common environmental factor that nuclear materials will encounter, both by chance, and by design. For example, uranium can be exposed to water from numerous research and application activities involving the nuclear fuel cycle and weaponization, which includes production of nuclear fuel, disposal of nuclear waste, atmospheric discharges from nuclear facilities, and accidental environmental releases.[6,7] Thus, the chemical fate of many uranium compounds is often dictated by their interactions with water. These interactions can produce crystal lattice hydration and hydrolysis resulting in changes to chemical form, crystallographic phase, and crystallinity.[5, 8]

Although thousands of unique uranium chemical structures can be found in the database of the International Centre for Diffraction Data (ICDD)[9], only a handful of these have relevance to the nuclear industry.[8, 10, 11] These include uranium metal, uranium fluorides (UF_6 and UF_4), uranyl fluoride (typically as a hydrated form with variable water content as $UO_2F_2 \bullet xH_2O$), various uranium oxides (UO_2, UO_3, and U_3O_8), and uranium ore concentrates such as ammonium and potassium diuranates.[8,12] Uranium tetrafluoride is of particular interest as it is a key intermediate in nuclear fuel production processes as a precursor to UF_6 – the key compound in the uranium enrichment process. Despite its close industrial connection to UF_6, many chemical properties of UF_4 are much less well characterized than its hexafluoride counterpart.

With regards to its interactions with water, UF_4 is sparingly soluble due to interactions between hydrogen in water and fluorine in the tetrafluoride compound. Water can also occupy vacancy sites of the U^{4+} ion to form two hydrate phases: the pseudo-cubic $UF_4(H_2O)_n$ where $0.5 \leq n \leq 2$ and $UF_4(H_2O)_{2.5}$.[13,14] The 2.5 hydrate, which has been minimally characterized to-date, has been shown to form when anhydrous UF_4 is placed in dilute aqueous HF solutions.[15,16] The pseudo-cubic phase, which is a derivative of the CaF_2-type phase, can form from a number of reactions, including electrolytic reduction of uranyl fluoride (UO_2F_2) in aqueous hydrofluoric acid,[17, 18] addition of aqueous hydrofluoric acid to aqueous uranium tetrachloride (UCl_4),[19] and hydration of UF_4 formed from various dehydration reactions.[13,14] One report has even shown that $UF_4(H_2O)_n$ might hydrate as low as n = 0.4.[20]

Elevated-temperature interactions of UF_4 and water produce a variety of compounds. In an atmosphere of water and nitrogen gas at 350 - 400 °C, UF_4 forms UO_{2+x} ($x \sim 0.3$). At the same temperature, in an atmosphere of water and oxygen, UF_4 forms U_3O_8 and UO_2F_2. Near 500 °C in an atmosphere of water and oxygen, U_3O_8 is formed.[16]

[a] Savannah River National Laboratory, Aiken, SC 29803
[b] Naval Research Laboratory, Washington, D.C. 20375
* Matthew.Wellons@srnl.doe.gov
‡Christopher.klug@nrl.navy.mil
§ Electronic Supplementary Information (ESI) available free of charge: [details of any supplementary information available should be included here]. See DOI: 10.1039/x0xx00000x

Historically, these reactions were presumed to be slow or non-existent at ambient laboratory temperatures. However, in 2015, Zhong *et al.* observed similar reactions at room temperature when samples of UF_4 were mixed with KBr to be monitored by infrared spectroscopy over a period of two months.[21] The KBr readily absorbed ambient moisture, thus providing the UF_4 with ample water to facilitate room temperature hydrolysis. UO_2F_2 and its hydrates were reported as the primary hydrolysis product, with U_3O_8, UO_2, and UO_3 appearing in small amounts with increased reaction time. Importantly, the amount of water exposure was loosely defined using this technique, and it is well known that solubility of a solid phase (in this case UF_4) can be altered by the addition of ligands (in this case K^+ and Br^-) to the contacting aqueous phase. For example, Wise et al. showed that uranium tetrafluoride dissolution is significantly enhanced in the presence of boric acid.[22] Similarly, PuF_4 has been shown to increase its water solubility in the presence of multiple cations, including B^{3+}, Al^{3+}, Th^{4+} and others. Conversely, PuF_4 can form insoluble compounds in the presence of aqueous cations like Ca^{2+} and Mg^{2+}.[23] Thus, UF_4 reactivity with water in the presence of KBr, may not be the same without KBr.

In historic studies, evaluation of UF_4 reactions with water have been contradictory. For example, a 1942 study showed that 85% of UF_4 degrades **wh**en placed in water for 24 hours; however, in the same study, no noticeable hydrolysis of UF_4 was observed when it was placed in boiling water for 72 hours.[24, 25] A 1961 review by Tananaev et al. highlights these and other inconsistencies pertaining to physiochemical reports of UF_4.[16] Interestingly, few reports on UF_4 physiochemical properties and its interactions with water have been published after the 1960s. Thus, most historical studies of UF_4 have never been repeated or re-analyzed using modern analytical instrumentation. A useful summary of many historical studies was produced by Grenthe et al. in 1992.[26]

Since global interests in uranium have shifted from pre-1970s weapons development to post-1970s nuclear nonproliferation, modern physiochemical data of UF_4 can be used in an entirely different way than historical data was used. For example, the field of nuclear forensics, which relies on identification of nuclear materials and their progeny to detect illicit nuclear activity, could benefit greatly from improved understanding of nuclear material physiochemical properties.[27,28] Furthermore, computational modeling to compliment modern physiochemical measurements might create new ways of understanding UF_4 and other important nuclear materials that have not been studied using modern techniques. [29,30]

The aforementioned UF_4 work by Zhong *et al.* in 2015 signified a potential paradigm shift with regards to UF_4-water interactions at room temperature since UF_4 was historically believed to be very stable under ambient environmental conditions. As such, it provided us with motivation to evaluate UF_4-water interactions at room temperature using several modern analytical tools.

Raman spectroscopy is a particularly useful characterization tool for evaluating UF_4 and the first high-resolution Raman spectrum of UF_4 was published only five years ago by our group at the Savannah River National Laboratory.[31] Symmetry analysis of UF_4 shows that over 42 optical modes should be Raman active,[29] and the published spectra show that many of those modes are measurable. In hindsight, previous Raman spectroscopic characterization attempts of UF_4 were complicated due to significant fluorescence at typical interrogating wavelengths (632 and 647 nm) and an overall weak UF_4 Raman signal intensity. However, at 325 and 785 nm, fluorescence is significantly reduced which enables the observation of multiple bands with strong intensity.

Fluorine-19 Nuclear Magnetic Resonance (NMR) is another tool that can be used to evaluate UF_4 and its interactions with water. Like Raman spectroscopy, few modern studies have been published on the NMR of UF_4 or the related uranyl fluoride.[32, 33] The lack of modern NMR data for UF_4 may be due to interactions between ^{19}F and paramagnetic U^{4+} ions, which lead to a broad, two-peak spectrum that cannot be separated into components corresponding to the multiple nonequivalent fluorine sites in UF_4. However, NMR of ^{19}F in UF_4 can still be informative for tracking chemical changes caused by reactions with water, particularly as U^{4+} ions convert to diamagnetic U^{6+} ions. Furthermore, a recent publication by our group described a high sensitivity low field automated detection technique that can be used to acquire broad NMR spectra for nuclei like ^{19}F in UF_4 and ^{195}Pt in platinum nanoparticles; this technique is suited for following chemical changes over long periods of time.[34]

With these recent developments in both NMR and Raman spectroscopy of UF_4, we postulated that it should be possible to use these techniques to probe for poorly understood interactions between UF_4 and water at room temperature; possibly leading to data to build a modern geochemical speciation model of this important nuclear compound. Room temperature UF_4-water interactions are perhaps the most pragmatic for environmental and nuclear nonproliferation research since the majority of both deliberate and accidental interactions between UF_4 and water are likely to occur under ambient environmental conditions.

Using a combination of ^{19}F NMR, Raman spectroscopy, infrared (IR) spectroscopy, powder X-ray diffraction (pXRD), and scanning electron microscopy (SEM), we show herein that UF_4 reacts with water at room temperature (20 – 23 °C) to primarily form crystalline $UF_4(H_2O)_{2.5}$. The Raman spectrum of $UF_4(H_2O)_{2.5}$ is published herein for the first time and is shown to be markedly different than the Raman spectrum of anhydrous UF_4, a result that is consistent with the two compounds having significantly different crystal structures.[35,15] Both Raman and IR spectral bands were deconvoluted with GRAMS/AI spectroscopy software. ^{19}F magic angle spinning (MAS) NMR confirms that a minor amount of $UO_2F_2(H_2O)_{1.57}$ is also formed from room temperature reactions between water and UF_4. Since UF_4 is an important compound used in many nuclear processes, the data presented herein should have implications in many nuclear fields, including nuclear nonproliferation, nuclear forensics, and environmental remediation, all of which benefit from an improved fundamental understanding of how solid state UF_4 particles transform in the presence of water near room temperature.

Results and Discussion

Commercially purchased anhydrous UF_4 was first analyzed via Raman spectroscopy, IR spectroscopy, and pXRD (SI Figures 1, 2, and 3 respectively). All three techniques confirmed the

commercial material to be anhydrous UF_4, with pXRD showing an excellent match to the ICDD diffraction pattern of UF_4 (Powder Diffraction File [PDF] No. 01-082-2317)[35, 36] and Raman measurements showing 16 distinct bands between 50 – 610 cm^{-1} that are characteristic of previously published spectra for anhydrous UF_4 (See Table 1).[31] These numerous Raman bands stem from UF_4 having a complex three-dimensional polymeric structure where uranium atoms in square-antiprismatic environments are bridged by fluorine atoms, similar to ZrF_4, HfF_4, and CeF_4.[37] For IR, the absence of resonance absorption is also consistent with anhydrous UF_4 since this compound has no active vibrational modes in the IR spectral range.[38,39]

Baseline characterization of anhydrous UF_4 was then measured using ^{19}F NMR (Figure 1). Paramagnetic U^{4+} causes the ^{19}F spin-lattice relaxation time, T_1, to be very short, thus permitting a delay of only 4 ms between scans and quick acquisition of spectra with good signal-to-noise. Spectra were obtained using both a point-by-point and automated method. In the point-by-point method, the spectrometer frequency was stepped from 93.8 MHz to 94.8 MHz with sub-spectra measured at each frequency. Each sub-spectrum was acquired using a two-pulse solid echo where each pulse was 0.8 µs in length, the time between pulses was 25 µs, and the total number of scans was 2048. The probe was re-tuned at each frequency and the final spectrum was constructed by combining all sub-spectra.

The automated method was devised to obtain a full spectrum over 1 MHz without the need to re-tune to each series of frequencies manually.[34] In the automated method, spectra were obtained with the spectrometer frequency and probe tuning fixed at 93.8 MHz while the probe itself was moved stepwise along the axis of the superconducting solenoid leading to a series of spectra obtained at a series of fields. Like the point-by-point method, each sub-spectrum was acquired using a two-pulse solid echo where each pulse was 0.8 µs in length, the time between pulses was 25 µs, the wait time between scans was 4 ms, and the total number of scans was 2048. In both approaches, the total ^{19}F NMR spectrum is obtained from the envelope of the subspectra as shown in Figure 2. The clear advantage of the automated method for this work is that it allows continuous acquisition of full spectra over long periods of time, e.g. days, ideal for monitoring slow changes.

Anhydrous UF_4 NMR spectra were similar in both the point-by-point and automated methods, as shown in Figure 1. The UF_4 NMR spectrum is a broad powder pattern which appears to contain two main features centered at 94.52 and 94.15 MHz with linewidths of 320 kHz and 150 kHz respectively. These features are consistent with our own prior measurements of UF_4 as well as results in the literature measured at different magnetic fields.[32-34] The asymmetric shape and significant broadening are due to the presence of paramagnetic U^{4+} and the large homonuclear dipolar coupling between many ^{19}F nuclei. Since the automated method allowed unattended repeated acquisition of the entire broad spectrum every 25 minutes, it was used in many of the subsequent measurements to follow changes with time.

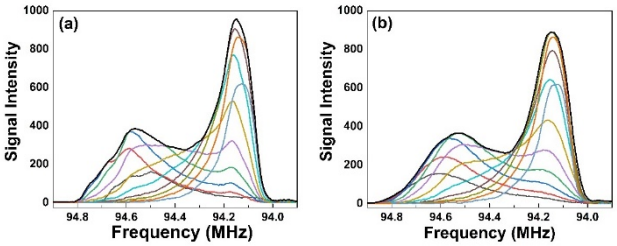

Figure 1. ^{19}F NMR spectra of anhydrous UF_4 obtained using a) point-by-point method and b) automated method. The sub-spectra obtained from 11 experiments with different frequencies (a) or 11 different probe heights (b) are shown as interior colored lines while the final total spectrum obtained from the envelope

Following baseline characterization of anhydrous UF_4, the material was placed in deionized water where it was agitated using magnetic stirring. Water exposed samples are hereafter referred to as "UF_4 hydrate". After one day of stirring in deionized water, there was a slight color change of the solid from emerald-green to blue-green, but the water remained colorless. Some of the solid material was removed, filtered, and dried for subsequent solid state analysis. Multiple UF_4-water mixing durations were tested, but in all cases between 1-6 days, the water remained colorless and the filtered product yielded a blue-green solid that was later determined by pXRD to be $UF_4(H_2O)_{2.5}$. When stirred for longer than 6 days, the color of the solid changed rapidly from blue-green to yellow. This color transformation was immediately followed by dissolution of the solids into a yellow solution and no further solid state analysis was feasible. A yellow color is typical for UO_2F_2 and schoepite ($(UO_2)_8O_2(OH)_{12}(H_2O)_{12}$), both of which are known to be soluble in water, and are therefore suspected to be the soluble products.[8] Because the purpose of this study was to characterize solid UF_4 particles and their transformation in the presence of room temperature water, liquid state analysis of chemical speciation was not within the scope of this study.

As shown in Figure 2, the X-ray diffraction pattern of UF_4 hydrate was markedly different than anhydrous UF_4 and showed an excellent match to the ICDD diffraction pattern of $UF_4(H_2O)_{2.5}$ (PDF No. 01-073-0736).[40, 41] This data makes it clear that anhydrous UF_4 forms $UF_4(H_2O)_{2.5}$ when stirred in water for 1 – 6 days. For reference, crystallographic structures of both UF_4 and $UF_4(H_2O)_{2.5}$ are shown in SI Figure 4 and specific crystallographic characteristics are listed in SI Table 1. Due to several overlapping peaks in the diffraction pattern of $UF_4(H_2O)_{2.5}$ with uranyl fluoride and several uranyl fluoride hydrates, particularly in the 25–45 2θ range, we could not find definitive evidence for uranyl compounds being present in the water exposed sample. This is likely because uranyl compounds are soluble and, if present, would have been removed from the sample after it was filtered following its exposure to water.

The Raman and IR spectra obtained on filtered solids of UF_4 hydrate are compared with the spectra of anhydrous UF_4 in Figure 3. As stated above, the UF_4 hydrate sample was confirmed by pXRD to be $UF_4(H_2O)_{2.5}$, thus, the presented Raman and IR data can be interpreted by comparison of the crystal structures of UF_4 and $UF_4(H_2O)_{2.5}$.

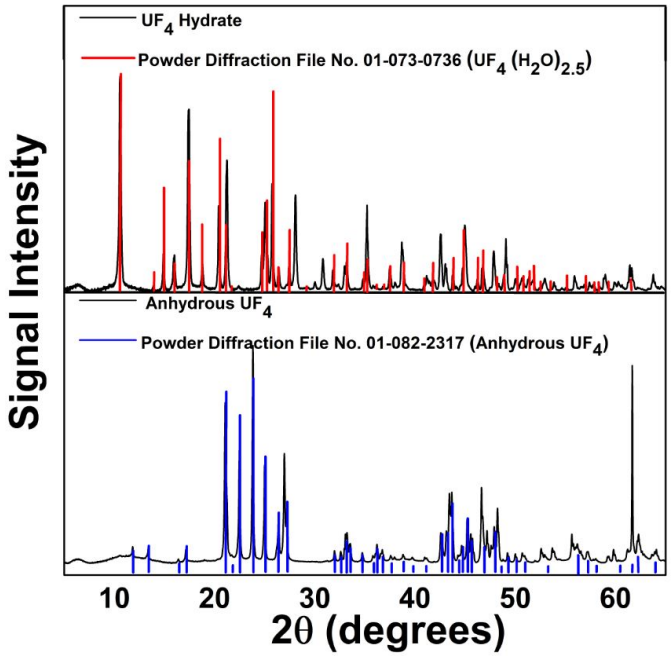

Figure 2. The powder X-ray diffraction pattern of UF_4 hydrate compared to our anhydrous UF_4 pattern and the ICDD powder diffraction data for anhydrous UF_4 and $UF_4(H_2O)_{2.5}$. The UF_4 hydrate pattern is an excellent match to the $UF_4(H_2O)_{2.5}$ pattern, thus indicating the UF_4 sample hydrated to $UF_4(H_2O)_{2.5}$ after 1-6 days in water.

Both the Raman and IR spectra of UF_4 and $UF_4(H_2O)_{2.5}$ were significantly different with the spectra of $UF_4(H_2O)_{2.5}$ being more complex than its anhydrous counterpart.

For Raman, the three-dimensional polymeric structure of UF_4 and $UF_4(H_2O)_{2.5}$ is evidenced via the numerous optical and acoustic vibrational modes in the low wavenumber (50 - 500 cm^{-1}) region of the spectra. Although numerous bands are identified for both compounds in this spectral region, there is little overlap in the band frequencies and there was no evidence for uranyl fluoride or schoepite in either spectra (Table 1). In total, 18 Raman bands were identified for $UF_4(H_2O)_{2.5}$ with intense bands at 118, 235, 427, and between 3000 - 3650 cm^{-1}. The high wavenumber (3000 – 3650 cm^{-1}) bands in the spectrum represent the OH spectral region and thus, no bands were anticipated or measured in this region for UF_4 but several were evident for $UF_4(H_2O)_{2.5}$. Generally, the high wavenumber Raman bands of $UF_4(H_2O)_{2.5}$ can be described as an agglomerate of bands stemming from both free and hydrogen bonded OH groups. This result is consistent with the crystal structure of $UF_4(H_2O)_{2.5}$ (SI FIGURE 4), which shows water molecules in the crystal lattice of $UF_4(H_2O)_{2.5}$, assumed by the position of oxygen within the lattice, can be classified as interstitial (free) or bonded to uranium.[15] GRAMS/AI software was used to deconvolute these Raman bands and four OH stretches were identified at 3535, 3480, 3390, and 3283 cm^{-1} with full-width half-maximum (FWHM) of 42, 61, 124, and 91 cm^{-1}, respectively (see Table 1). The correlation number between the measured spectrum and the simulated fit was 0.9949 with a standard error of 1.86 that is likely this high due to noise in the spectrum.

The IR spectrum of anhydrous UF_4 was unremarkable due to the compound having no active vibrational modes in the measured spectral range; however, several resonance bands were observed for $UF_4(H_2O)_{2.5}$. As shown in Table 1, our IR spectrum of $UF_4(H_2O)_{2.5}$ is mostly consistent with a previously published spectrum of this compoud.[42] In the high frequency OH stretch region of the IR spectrum, $UF_4(H_2O)_{2.5}$ produced an agglomerate of bands that were well fit into 6 bands using GRAMS/AI software. The sharpest band in this region (3539 cm^{-1}) is likely due to free OH since free OH has a higher resonance frequency than hydrogen bound OH. In the mid-frequency HOH bending range, $UF_4(H_2O)_{2.5}$ produced three IR bands. These three bands suggest there at least three water molecules with differing local environments in the crystal lattice of $UF_4(H_2O)_{2.5}$ and is consistent with the material's crystal structure. Several IR bands were identified at low frequency and are likely produced by multiple bond formations between H_2O and UF_4. Like Raman measurements, there was no evidence for uranyl fluoride or schoepite in the IR spectra of either UF_4 or $UF_4(H_2O)_{2.5}$.

In general, differences in the Raman and IR of UF_4 and $UF_4(H_2O)_{2.5}$ can be attributed to the significant dissimilarities of the crystal structures of these compounds. For example, while UF_4 has a monoclinic unit cell with the C2/c space group, $UF_4(H_2O)_{2.5}$ has a rhombic unit cell with Pnam space group. UF_4 forms a UF_8 polyhedron within a unit cell whereas $UF_4(H_2O)_{2.5}$ forms a UF_9 polyhedron. The uranium nonahedron of $UF_4(H_2O)_{2.5}$ form bands along the crystallographic c axis and the three-dimensional framework formed by these bands are filled by water molecules.

While the structure and vibrational modes of anhydrous UF_4 can be better understood by comparison with well-characterized isostructural compounds like ZrF_4 and HfF_4,[37] the hydrates of these tetrafluoride compounds can vary in their crystal structure and hydration levels, thus making complete interpretation of the $UF_4(H_2O)_{2.5}$ vibrational spectra challenging. For example, the trihydrate of HfF_4 possess a monoclinic polymeric structure while ZrF_4 possesses a triclinic polymeric structure; neither of these compounds are known to form a 2.5 hydrate like UF_4.[43,44] Attempts to understand the factors underlying the stoichiometry and structural differences between metal tetrafluoride hydrates, particularly HfF_4 and ZrF_4, were made by Rickard and Waters with the assumption that atomic size, fluorine bridging, hydrogen bonds, lattice voids, and basicity play important roles in determining stoichiometry and structure.[45] Unfortunately, little understanding was gained as to why the hydrate structures of these tetrafluoride compounds differ.

The hydrates of ThF_4 and PuF_4 might be expected to be isostructural to UF_4 since the anhydrous forms of these compounds are isostructural; however, $ThF_4(H_2O)_{2.5}$ is pseudo-tetragonal while the 2.5 hydrates of UF_4 and PuF_4 are both rhombic.[46] Thus, to the best of our knowledge, it seems that PuF_4 and its hydrates may be the best compounds to compare structure and vibrational modes with UF_4 and its hydrates. Unfortunately, the Raman spectra of PuF_4 and its hydrates have never been published; likely due to the significant radiological hazards associated with handling plutonium. One method that might be useful in better assignment of the vibrational modes of $UF_4(H_2O)_{2.5}$ is density functional perturbation theory with on-site Coulomb corrections to calculate phonon normal modes, IR

intensity, and Raman activity, as was recently done by Miskowiec et al. for UF_x with x = 3, 4, 4.5, and 5.[29]

Table 1. Raman and IR resonance bands identified for anhydrous UF_4 and UF_4 hydrate. Raman and IR bands are labeled with an (R) or (IR), respectively. Anhydrous UF_4 Raman band positions are compared with the anhydrous UF_4 spectrum measured by Villa-Aleman and Wellons.[31] The IR spectrum of anhydrous UF_4 has no vibrational modes in the measured spectral region. The IR modes of UF_4 hydrate are categorized based on their likely identity (e.g., O-H, H_2O, H_2O/F, and U-F). UF_4 hydrate band positions are compared with the $UF_4(H_2O)_{2.5}$ spectrum measured by Khanaev et al.[42] to show that our UF_4 hydrate spectrum is mostly consistent with an assignment of $UF_4(H_2O)_{2.5}$.

Anhydrous UF_4 Raman (R) Band Positions (cm^{-1})		**UF_4 Hydrate** Raman (R) and Infrared (IR) Band Positions (cm^{-1})	
This work	Villa-Aleman[31]	This work	$UF_4(H_2O)_{2.5}$ [42]
4300 (R)			
		3539 (IR) O-H	3540 (IR) O-H
		3535 (R)	
		3481 (R)	
		3470 (IR) O-H	
		3390 (R)	
		3385 (IR) O-H	
		3313 (IR) O-H	3385 (IR) O-H
		3283 (R/IR)	
		3218 (IR) O-H	3230 (IR) O-H
		3117 (IR) O-H	3110 (IR) O-H
		1666 (IR) H_2O	1655 (IR) H_2O
		1637 (IR) H_2O	1634 (IR) H_2O
		1599 (IR) H_2O	1600 (IR) H_2O
		790 (IR) H_2O/F	
		737 (IR) H_2O/F	
		640 (IR) H_2O/F	645 (IR) H_2O/F
604 (R)	603.6 (R)		
		590 (IR) H_2O/F	
		547 (IR) H_2O/F	550 (IR) H_2O/F
		486 (IR) H_2O/F	
		440 (IR) H_2O/F	430 (IR) H_2O/F
		427 (R)	
		405 (IR) U-F	400 (IR) U-F
361 (R)	360.8 (R)	364 (R)	
		340 (R)	
		333 (R)	
322 (R)	322.4 (R)	320 (R)	
296 (R)	296.1 (R)		
		282 (R)	
256 (R)	255.8 (R)	257 (R)	
		235 (R)	
197 (R)	197.3 (R)		
		185 (R)	
170 (R)	170.4 (R)		
		156 (R)	
149 (R)	148.5 (R)		
131 (R)	131.4 (R)		
		118 (R)	
116 (R)	115.9 (R)		
107 (R)	107.2 (R)	106 (R)	
101 (R)	101.3 (R)		
		95 (R)	
91 (R)	91.0 (R)		
79 (R)	78.9 (R)	82 (R)	
67 (R)	66.8 (R)		
60 (R)	59.4 (R)		

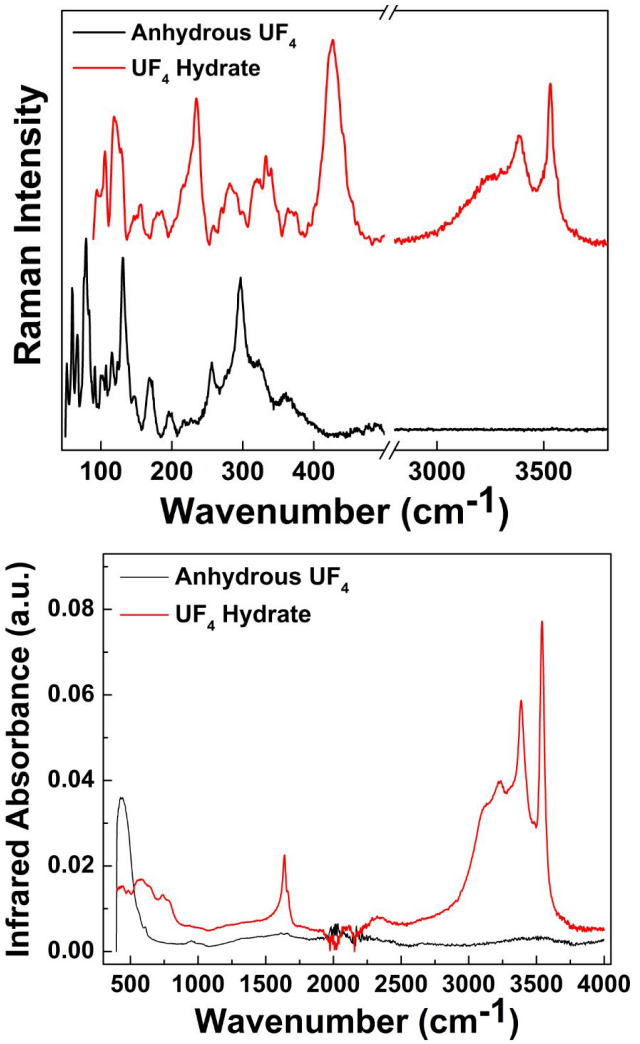

Figure 3. Left: Raman spectrum of UF4 hydrate (red trace) compared with the spectrum of anhydrous UF4 (black trace). Both spectra were acquired with a 785 nm excitation laser. Right: Infrared spectrum of anhydrous UF4 (black trace) and UF4 hydrate (red trace). The black trace is unremarkable, which is consistent with anhydrous UF4 having no vibrational modes in the measured IR spectral range. The red trace has multiple identifiable bands that are consistent with previously published measurements of UF4(H2O)2.5.[42] The sharp feature near 500 cm-1 is fluorescence and the sharp features between 2000 - 2200 cm-1 are artifacts of the diamond ATR in the spectrometer.

In a separate parallel series of experiments, NMR spectra were then measured for UF_4 while it resided in deionized water. The spectrum immediately changed upon water exposure, as shown in Figure 4a and 4b. The most prominent spectral change occurred at the high frequency edge of the spectrum which decreased in intensity. Over the next three days, the only further change was a minor reduction in the intensity of the feature near 93.35 MHz. These measurements were all carried out using the automated approach, which can make it difficult to observe small contributions from narrow peaks due to the variation in field homogeneity over the sample as a function of probe height.

After the sample had soaked in water for four days, and it appeared that the spectra had reached a steady state, a measurement was performed at a probe height where the field homogeneity was optimal and at a frequency where fluorine bound to diamagnetic species (e.g., U^{6+}) is likely to be observed. Under these measurement parameters, a very low intensity,

relatively narrow peak of width less than 0.1 MHz was observed at ~ 94.36 MHz. The narrow peak contained a small shoulder at ~ 94.3 MHz and the integrated intensity of the entire narrow peak represented less than 3% of the total integrated intensity of the spectrum; which itself is a sub-spectrum of the total ^{19}F NMR spectrum. The position of the narrow peak and its shoulder are consistent with fluorine in uranyl fluoride and fluorine bonded to carbon respectively. The fluorine-carbon bonds are believed to have formed when HF, generated from the UF_4-water reaction (vide infra), reacted with the polyethylene sample holder. SI Figure 5 highlights similarities between the narrow peak and the spectrum of commercial $UO_2F_2(H_2O)_{1.57}$ obtained under the same measurement conditions. These data indicate that a small amount of $UO_2F_2(H_2O)_{1.57}$ forms when UF_4 is placed in water for several days. Subsequently, a small aliquot of solid sample was removed from the water and was further analyzed by ^{19}F MAS NMR to confirm the formation of $UO_2F_2(H_2O)_{1.57}$ (SI Figures 6 and 7).

After more than one year, we returned to the same material and obtained full ^{19}F NMR spectra using the point-by-point method to ensure maximal resolution. By this time, the sample appeared dry with only a hard clump remaining. The ^{19}F spectra shown in Figures 4c and 4d are clearly very different from those observed for the initial material (i.e., **Figure 1**). Also shown in Figure 4 are spectra measured for $UF_4(H_2O)_{2.5}$ which was made in a separate experiment by mixing UF_4 and water followed by filtration and air drying (Figures 4e and 4f). There is clearly good agreement between the aged UF_4-water spectrum and $UF_4(H_2O)_{2.5}$. Note, the spectrum in Figure 4e contains a peak suggestive of the presence of a UO_2F_2[47]. These results support our claim that UF_4 ultimately forms $UF_4(H_2O)_{2.5}$ when placed in water and it seems that minor amounts of soluble UO_2F_2 can also form. These results also highlight the advantages of performing ^{19}F NMR instead of ^{1}H NMR to probe UF_4-water interactions. Although ^{1}H NMR has slightly higher sensitivity, ^{19}F NMR has greater selectivity in this case and is better able to probe uranium interactions and oxidation state since fluorine is bonded directly to the uranium whereas ^{1}H spectra would only probe mobile water and therefore only represent an average environment around the uranium species of interest.

It is important to note that hydration of UF_4 to $UF_4(H_2O)_{2.5}$ occurred slower during NMR analysis compared to Raman, IR, and pXRD analysis. This discrepancy is likely attributed to differences in how samples were prepared for these measurements, and (to a lesser extent) differences in the structural information that is probed by these different techniques. With regards to sample preparation, Raman, IR, and pXRD measurements were not be obtained while UF_4 was in water. Thus, these measurements were made after our uranium sample was filtered after stirring in water for 1 - 6 days. Conversely, NMR measurements were obtained while UF_4 resided in water since the presence of an abundance of water did not interfere with these measurements. Therefore, NMR spectra were obtained while UF_4 resided in water; however, the sample could not be agitated or stirred while inside the small polyethylene NMR sample holder. It is likely that the stirring of UF_4 in water for Raman, IR, and pXRD measurements increased the formation rate of $UF_4(H_2O)_{2.5}$ relative to NMR measurements where UF_4 passively resided in water. Importantly, if soluble uranyl fluoride formed during experiments where samples were filtered and dried (Raman, IR, pXRD), then it would have been removed prior to solid state analyses. This fact is likely why uranyl fluoride was only observed during *in situ* NMR measurements. Nonetheless, the formation of uranyl fluoride appears to be very minimal and it is clear that $UF_4(H_2O)_{2.5}$ is the primary hydrolysis product of UF_4.

With regards to differences in the structural information probed by each analytical technique, NMR provides bulk information whereas Raman and IR are more sensitive to a sample surface. Since it is likely that hydration first occurred on the surface of analyzed particles, it is reasonable to assume that Raman and IR measurements would indicate hydration more readily than NMR measurements; however, pXRD is also a bulk measurement, and diffraction data also indicated rapid hydration like Raman and IR measurements. Thus, differences in sample preparation (stirring versus not stirring) likely caused the observed differences in the rate of formation of $UF_4(H_2O)_{2.5}$.

One advantage of the *in situ* NMR measurements is that both UF_4 and water were confined to the sample vial throughout our experiments. These measurements allowed us

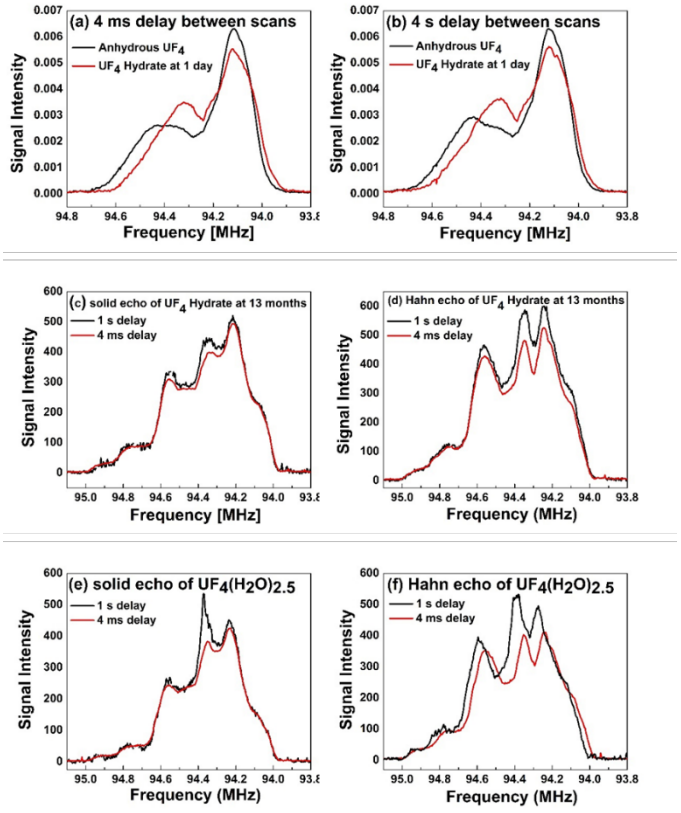

Figure 1. ^{19}F NMR spectra of anhydrous UF_4 and UF_4 hydrate at 1 day in H_2O with (a) a delay time between scans of 4 ms and (b) a delay time between scans of 4 s. The spectra in (a) are normalized to have equal total areas; identical scaling factors were applied to (b). Parts (c) and (d) show ^{19}F spectra obtained using the point-by-point method for UF_4 hydrate after thirteen months of water exposure using either (c) solid echo or (d) a Hahn echo sequence. Parts (e) and (f) show ^{19}F spectrum of commercial $UF_4(H_2O)_{2.5}$ obtained using (e) the point-by-point method and a solid echo or (f) a Hahn echo sequence. Note that spectrum (e) contains a small peak just below 94.4 MHz which is suggestive of the presence of UO_2F_2.

to observe the UF_4 hydrate spectrum evolve with time, thereby revealing the minor formation of uranyl fluoride, which was not observed in Raman, IR, or pXRD analyses since it was likely removed via filtration prior to these analyses. As an aside, we suspect that UF_4 particles with a larger surface-to-volume ratio might have formed $UF_4(H_2O)_{2.5}$ and UO_2F_2 more readily when exposed to water due to increased surface area for interactions.

Scanning electron micrographs were obtained to further understand the evolution of UF_4 in water. Particle size dispersity and morphology were analyzed and showed that pristine UF_4 particles have spheroid morphology, a smooth surface, and diameters that ranged from approximately 3 µm up to 30 µm (Figure 5 top). Particle size is an important, but often overlooked parameter when studying chemical speciation; however, surface area will impact the extent of a particle's interactions with its environment. Specifically, larger surface area materials (i.e., small particles) would be expected to experience more interactions with their environment than low surface area materials (i.e., large particles). After stirring in water for 1 day to form $UF_4(H_2O)_{2.5}$, the morphology of our samples changed drastically to needle-like crystals with an appearance similar to previous descriptions of uranium fluoride hydrate crystals (Figure 5 bottom).[48] Importantly, we believe this SEM data may give some clue about the formation mechanism of $UF_4(H_2O)_{2.5}$. Although details surrounding the gross morphology change from spheres to needle-like crystals are not known, the change appears consistent with a bulk scale dissolution and reprecipitation process such as those demonstrated with typical nanoparticulate syntheses.

Prior to 2015, room temperature reactions between UF_4 and water were likely assumed to be either slow or non-existent. Zhong et al. showed this is not true by using infrared spectroscopy to demonstrate that room temperature hydrolysis of UF_4 can produce UO_2F_2 hydrates with U_3O_8, UO_2, and UO_3 formed in small amounts.[21]

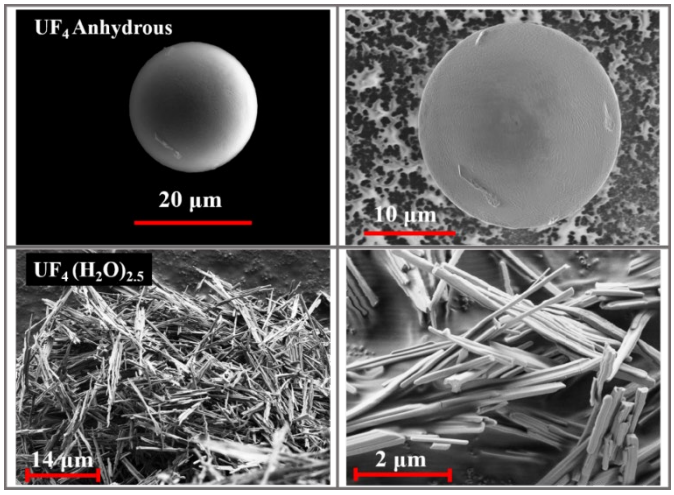

Figure 2 Top: SEM micrographs of anhydrous UF_4 before water exposure show that the pristine particles have spheroid morphology and a smooth surface. Bottom: SEM micrographs of UF_4 hydrate ($UF_4(H_2O)_{2.5}$) show that the particles form needle-like crystals.

However, it cannot be overlooked that these experiments were conducted in the presence of KBr which could have altered the reactions between UF_4 and water; furthermore, the water exposure variable was loosely defined in that study. After rigorous characterization using several different analytical techniques, we show herein that room temperature reactions between UF_4 and water not only exist but produce well-defined $UF_4(H_2O)_{2.5}$ with minor formation of soluble uranyl fluoride.

Assuming both oxygen and water react with UF_4, a balanced chemical equation describing the formation of UO_2F_2 from anhydrous UF_4 would be: $2UF_4 + O_2 + 2(H_2O) \rightarrow 2UO_2F_2 + 4HF$. It is also possible that UO_2F_2 might form from $UF_4(H_2O)_{2.5}$ or some transient uranium tetrafluoride hydrate, $UF_4(H_2O)_x$. In this case, one possible balanced chemical equation describing this formation would be: $2UF_4(H_2O)_x + O_2 \rightarrow 2UO_2F_2 + 4HF + 2|1-x|H_2O$. Note, this equation is invalid when $x = 0$ and UF_4 was recently shown by Pointurier et al. to be stable in dry air.[49] Although it is currently unclear if $UF_4(H_2O)_x$ would also be stable in dry air, we suspect that water, and oxygen liberated from water, are more important towards the formation of UO_2F_2 than atmospheric oxygen.

Importantly, NMR measurements showed that UO_2F_2 was detected before $UF_4(H_2O)_{2.5}$, which suggests a direct conversion of UO_2F_2 from UF_4. However, additional conversion of UO_2F_2 from $UF_4(H_2O)_{2.5}$ cannot be ruled out, especially because prolonged stirring of UF_4 in water eventually resulted in complete dissolution into a yellow solution that we suspect was a uranyl species.

While our NMR experiments certainly confirm the existence of a reaction pathway to generate UO_2F_2 from the room temperature reaction of UF_4 and water, we clearly show in all characterization techniques that $UF_4(H_2O)_{2.5}$ is the primary hydrolysis product for this reaction. This hydrated compound may form in the following single-step reaction: $2UF_4 + 2.5\ H_2O \rightarrow UF_4(H_2O)_{2.5}$.

When anhydrous UF_4 is stirred in water for 1 - 6 days, the abundance of water and agitation seemingly drives the formation of $UF_4(H_2O)_{2.5}$ with minimal or no side-products formed. When this reaction is not agitated, as was the case in our NMR experiments, it takes longer to form $UF_4(H_2O)_{2.5}$ and a minor amount (<5 % of the total sample) of uranyl fluoride also forms. Our discovery of uranyl fluoride bolsters the work by Zhong et al.[21], who also showed its formation from water-exposed UF_4; however, in contrast to the work by Zhong et al., no uranium oxides were found in this study. We postulate that reactions between UF_4 and water involve a complex interplay between water content and uranium particle surface. Therefore, it may be fruitful for future studies to investigate reactions between UF_4 and ambient humidity, especially humidity levels that might be encountered in a nuclear facility storing UF_4. Future work might also seek to utilize computational methods (e.g., DFT) to relate the $UF_4(H_2O)_{2.5}$ structure to the Raman observables, as was done recently for UO_3.[30] For our part, neutron scattering experiments are planned to further evaluate UF_4 interactions with water. Inelastic neutron scattering can provide insight into the number of water binding sites by locating splitting in O-H stretch and bending modes, as well as provide an assessment of the strength of hydrogen bonding within the structure.

Conclusions

Room temperature reactions between UF_4 and water were studied using multiple solid-state techniques. When anhydrous UF_4 is placed in water with agitation, it hydrates to $UF_4(H_2O)_{2.5}$ within 1 day. When placed in water without agitation, it takes significantly longer for $UF_4(H_2O)_{2.5}$ to form (possibly up to 13 months). $UF_4(H_2O)_{2.5}$ was rigorously characterized both structurally and spectroscopically, and in the case of Raman, was spectroscopically characterized for the first time on record. A minor amount of uranyl fluoride was also found to form via the UF_4-water reaction, but this species can elude detection by most solid-state techniques since the compound is soluble in water. All results presented herein were verified using Raman, IR, and NMR spectroscopy, powder X-ray diffraction, and scanning electron microscopy. Future work is planned to investigate reactions of UF_4 and water at varying levels of ambient humidity and with neutron scattering measurements.

Experimental Methods

General Considerations

Caution: *The UF_4 in these experiments contains natural uranium. Standard precautions for handling radioactive materials are recommended.*

Anhydrous UF_4 was purchased from International Bio-Analytical Industries, Inc. and was stored in a temperature and humidity-controlled storage chamber (<10% relative humidity) to minimize contact with atmospheric water. The commercial material has a vibrant, emerald-green color. Purity and material phase were confirmed by powder X-ray diffraction (pXRD) upon receipt.

UF_4-water Experiments

To evaluate UF_4-water interactions, anhydrous UF_4 (100 mg, 0.32 mmol) was placed in 25 mL of deionized water (1.4 mol) and was agitated using magnetic stirring at a rate of approximately 100 revolutions per minute. After a day of stirring, the remaining solids were filtered at room temperature and were dried by passing room temperature air through the solids for one hour. The solids were immediately evaluated via Raman, IR, pXRD, and SEM. Multiple UF_4-water mixing durations were tested and the products in each case were characterized by pXRD. In all cases when mixing was between 2-6 days, the filtered product yielded $UF_4(H_2O)_{2.5}$.[50] Product yield declined with mixing beyond 6 days with eventual dissolution of all solid at 7 days.

For NMR experiments, UF_4 (50 mg, 0.16 mmol) was placed in a 0.3 mL polyethylene PELCO mini vial containing 0.2 mL deionized water (0.011 mol); *in situ* NMR measurements in water were then conducted. *In situ* measurements with water could not be conducted for IR or pXRD due to measurement interference from water, and they were not performed for Raman due to overlap of water bands with the characteristic low frequency (50 -450 cm^{-1}) UF_4 bands.

Nuclear Magnetic Resonance.

Most of the ^{19}F NMR spectra and relaxation rates were obtained for UF_4 under static (*i.e.*, non-spinning) conditions at room temperature and low field (2.35 T, ^{19}F resonance frequency of roughly 94.1 MHz) using specially designed sample holders and a homebuilt probe with a 3-turn RF coil and diameter of 7 mm which allowed for measurements during *in situ* exposure to water. Pulse lengths of the homebuilt probe were calibrated for optimal signal excitation and detection. All experiments were performed using an Oxford superconducting magnet with a maximum field of 2.35 T and a 110 mm diameter room temperature bore. The specially designed NMR probe was attached to a Thorlabs linear translation stage (LNRS/M) which was mounted vertically underneath the magnet. LabVIEW software (National Instruments) in combination with a Thorlabs stepper motor controller (BSC201) was used to control the vertical motion of the NMR probe. The NMR spectrometer was based on a Tecmag Redstone console. High power RF pulses were obtained via an AR 1000LPM8. The preamp was a Miteq AU-1313. ^{19}F NMR calibration using liquid hexafluorobenzene was achieved via a two-pulse Hahn echo experiment where the second pulse length was held fixed at 1.6 μs while the length of the first pulse was varied. Each data point was the sum of 128 scans with a wait time between scans of 8s. The ^{19}F NMR resonance frequency was 94.31 MHz. Optimal pulse lengths were determined from these data.

Raman Spectroscopy

Raman spectra were acquired on a LabRAM HR800 UV (Horiba Jobin-Yvon) equipped with a Newton EMCCD (Andor 970N-UVB) detector with a 1600 × 200 pixel array and 16 μm pixel resolution. Most experiments were conducted by binning the spectral array with a factor of two. The Andor detector was cooled to -95 °C with the help of a water chiller. Labspec 5.78 software was used to control the spectrometer and detector. The software was also used to conduct data manipulations. The excitation laser wavelength was λ = 785 nm. A 600 and an 1800 g/mm grating were used in the visible spectral range. Ultra-steep long pass edge filters acquired from Semrock Inc. were used to interrogate the vibrational spectra as close as 50 cm^{-1} of the laser excitation line. The laser power used in these experiments ranged from 100 μW to 2 mW. The laser intensity at the sample was controlled with neutral density filters and the microscope objective selection (primarily 100x). Laser power, microscope objective, pixel binning, grating and wavelength spectral region (fluorescence background) contributed to the integration time used during the acquisition of the Raman spectra. The integration time varied from a few seconds to several hours for a high signal to noise ratio. For each integration time, at least two spectra were co-added to remove the contribution of cosmic rays to the spectra. The spectral bands were analyzed and deconvoluted with GRAMS/AI spectroscopy software by Thermo Scientific.

Infrared Spectroscopy

A Nicolet 6700 Fourier transform infrared spectrometer equipped with an attenuated total reflectance (ATR) accessory and a DTGS detector was used for infrared spectroscopy measurements. Spectra were measured with a 4 cm^{-1} resolution. A total of 128 spectra were co-added during the acquisition and were recorded in the 400 to the 4000 cm^{-1} spectral window. Note, the spectral region 2000-2200 cm^{-1} demonstrates no measurable signal due to the diamond ATR accessory. The spectral bands were analyzed and deconvoluted with GRAMS/AI spectroscopy software by Thermo Scientific.

Powder X-ray Diffraction

Powder X-ray diffraction (pXRD) measurements were acquired using a Rigaku Ultima IV powder X-ray diffractometer. X-rays were produced from a copper target at 40 kV and 44 mA. Scattered X-rays were detected using a D/teX Ultra semi-conductor detector with a Cu Kβ filter, with the tube/detector operated in the focusing beam (Bragg Brentano) method. The divergence slit was set at 2/3° with a divergence height limit slit at 10 mm and the scattering slit set at 8.0 mm with the receiving slit open on the diffracted side of the beam. The sample substrate was a 1 inch silicon disk cut along the (510) crystal plane to minimize background reflections. Paraffin wax was used to secure the powders to the disk. The 2θ scan range was from 5 - 80° at a scan rate of 0.1° per minute. Measurements were performed with a stationary sample holder. XRD scans were analyzed with PDXL (Rigaku). A qualitative analysis of diffraction patterns was performed using search-match identification of the experimental XRD pattern to the ICDD database of crystal and powder X-ray diffraction pattern using the peak intensity and peak position.[9]

Scanning Electron Microscopy

A Zeiss Supra 40 VP FEG-SEM utilizing SmartSEM software acquired the included micrographs under high-vacuum conditions. High resolution microscopy analyses consisted of secondary electron detection with the standard 30 µm aperture. Images were obtained at magnifications ranging from 600 – 21,000x with accelerating voltages ranging from 1.0 – 20.0 kV.

Conflicts of interest

There are no conflicts to declare.

Acknowledgements

This work was supported by the Laboratory Directed Research and Development (LDRD) program within the Savannah River National Laboratory (SRNL). This document was prepared in conjunction with work accomplished under Contract No. DE-AC09-08SR22470 with the U.S. Department of Energy (DOE) Office of Environmental Management (EM).

Author Contributions

The manuscript was written through contributions of all authors. All authors have given approval to the final version of the manuscript.

ORCID Identifiers

Jonathan H. Christian: 0000-0003-1967-4841
Christopher A. Klug: 0000-0002-2752-7342
Michael DeVore II: 0000-0002-1770-4472
Eliel Villa-Aleman: 0000-0002-2891-0861
Bryan J. Foley: 0000-0003-0570-769X
Nicholas Groden: 0000-0003-1033-1236
A. Taylor Baldwin: 0000-0002-0259-4258
Matthew S. Wellons: 0000-0002-7172-2006

Notes and references

1. Development and Implementation Support Programme for Nuclear Verification 2018-2019. International Atomic Energy Agency, 2018., *Journal*.
2. M. J. Kristo, A. M. Gaffney, N. Marks, K. Knight, W. S. Cassata and I. D. Hutcheon, *Annual Review of Earth and Planetary Sciences*, 2016, **44**, 555-579.
3. D. Féron, in *Nuclear Corrosion Science and Engineering*, ed. D. Féron, Woodhead Publishing, 2012, pp. 31-56.
4. M. Said and A. E. Hixon, *Journal of Alloys and Compounds*, 2021, **854**, 156277.
5. M. C. Kirkegaard, M. W. Ambrogio, A. Miskowiec, A. E. Shields, J. L. Niedziela, T. L. Spano and B. B. Anderson, *Journal of Nuclear Materials*, 2020, **529**, 151889.
6. A. B. Kersting, *Inorganic Chemistry*, 2013, **52**, 3533-3546.
7. R. Kips, A. Leenaers, G. Tamborini, M. Betti, S. Van den Berghe, R. Wellum and P. Taylor, *Microscopy and Microanalysis*, 2007, **13**, 156-164.
8. D. L. Clark, S. S. Hecker, G. D. Jarvinen and M. P. Neu, *The Chemistry of the Actinide and Transactinide Elements*, Springer, Dordecht, 3rd edn., 2010.
9. S. Gates-Rector and T. Blanton, *Powder Diffraction*, 2019, **34**, 352-360.
10. P. G. Alfredson, *Chemical Technology Division, AAEC (Australian Atomic Energy Commission*, 1973 est., VIII-1 to VIII-22.
11. F. Kitts, *Pilot-scale demonstration of the modified direct denitration process to prepare uranium oxide for fuel fabrication evaluation*, Oak Ridge National Lab., 1994.
12. C. R. Edwards and A. J. Oliver, *JOM*, 2000, **52**, 12-20.
13. V. V. Bakakin, Y. V. Gagarinskii, S. V. Borisov, G. M. Zadneprovskii and S. A. Durasova, *Journal of Structural Chemistry*, 1965, **6**, 536-539.
14. J. K. Dawson, R. W. M. D'Eye and A. E. Truswell, *Journal of the Chemical Society (Resumed)*, 1954.
15. G. M. Zadneprovskii and S. V. Borisov, *Journal of Structural Chemistry*, 1972, **12**, 761-769.
16. I. V. Tananaev, N. S. Nikolaev, Y. A. Luk'yanychev and A. A. Opalovskii, *Russian Chemical Reviews*, 1961, **30**, 654-671.
17. J. R. Higgins, J. T. Roberts, C. W. Hancher and M. J. A, *Ind. Eng. Chem.*, 1958, **50**, 285.

18. W. W. Schulz, E. W. Neuvar, J. L. Caroll and R. E. Burns, *Ind. Eng. Chem.*, 1958, **50**, 1768.
19. H. C. Bolton, *Bull. Soc. chim. France*, 1866, **2**, 450.
20. Y. V. Gagarinskii and V. P. Mashirev, *Russ. J. Inorg. Chem.*, 1959, **4**, 565.
21. J. Zhong, S. Lang and Y. Chunrong, *Acta Physico-Chimica Sinica (in Chinese)*, 2015, **31**, 2251-2258.
22. W. M. Wise, H. R. Soehnlin and C. H. McBride, *Analytical Chemistry*, 1962, **34**, 1035-1035.
23. J. D. Navratil, *Journal of Inorganic and Nuclear Chemistry*, 1969, **31**, 3676-3680.
24. A. Roberts, *Report B-64, Cited in the book by J. Katz and E. Rabinowich. The Chemistry of Uranium [Russian translation] Moscow, Foreign Literature Press, 1954.*
25. N. S. Nikolaev and Y. A. Luk'yanychev, *The Soviet Journal of Atomic Energy*, 1962, **11**, 704-706.
26. K. H. Lieser, *Berichte der Bunsengesellschaft für physikalische Chemie*, 1993, **97**, 148-148.
27. K. Mayer, M. Wallenius and Z. Varga, *Chemical Reviews*, 2013, **113**, 884-900.
28. A. Miskowiec, J. L. Niedziela, M. C. Kirkegaard and A. E. Shields, *Scientific Reports*, 2019, **9**, 10476.
29. A. Miskowiec, A. E. Shields, J. L. Niedziela, Y. Cheng, P. Taylor, G. DelCul, R. Hunt, B. Spencer, J. Langford and D. Abernathy, *Physica B: Condensed Matter*, 2019, **570**, 194-205.
30. T. L. Spano, A. E. Shields, B. S. Barth, J. D. Gruidl, J. L. Niedziela, R. J. Kapsimalis and A. Miskowiec, *Inorganic Chemistry*, 2020, **59**, 11481-11492.
31. E. Villa-Aleman and M. S. Wellons, *Journal of Raman Spectroscopy*, 2016, **47**, 865-870.
32. S. P. Gabuda, L. G. Falaleeva and Y. V. Gagarinskii, *Physica Status Solidi (b)*, 1969, **33**, 435-438.
33. M. Pintar, *Physica Status Solidi (b)*, 1966, **14**, 291-295.
34. C. A. Klug and J. B. Miller, *Solid State Nuclear Magnetic Resonance*, 2018, **92**, 14-18.
35. S. Kern, J. Hayward, S. Roberts, J. W. R. Jr., F. J. Rotella, L. Soderholm, B. Cort, M. Tinkle, M. West, D. Hoisington and G. H. Lander, *The Journal of Chemical Physics*, 1994, **101**, 9333-9337.
36. PDF 4 Database, International Centre for Diffraction Data, Newtown Square, PA, 2015, Card No #01-082-2317.
37. M. Goldstein, R. J. Hughes and W. D. Unsworth, *Spectrochim. Acta, Part A. 1975, 31A, 621.*
38. K. R. Kunze, R. H. Hauge, D. Hamill and J. L. Margrave, *The Journal of Physical Chemistry*, 1977, **81**, 1664-1667.
39. R. J. M. Konings, A. S. Booij, A. Kovács, G. V. Girichev, N. I. Giricheva and O. G. Krasnova, *Journal of Molecular Structure: THEOCHEM*, 1996, **378**, 121-131.
40. S. V. Borisov and G. M. Zadneprovskii, *Soviet Atomic Energy*, 1971, **31**, 761-763.
41. PDF 4 Database, International Centre for Diffraction Data, Newtown Square, PA, 2015, Card No #01-073-0736.
42. E. I. Khanaev, E. G. Teterin and L. A. Luk'yanova, *Journal of Applied Spectroscopy*, 1967, **6**, 533-538.
43. S. K. Dey, C. C. Dey and S. Saha, *Journal of Physics and Chemistry of Solids*, 2016, **91**, 18-24.
44. A. Lerf and T. Butz, *Hyperfine Interactions*, 1987, **36**, 275-370.
45. C. E. F. Rickard and T. N. Waters, *Journal of Inorganic and Nuclear Chemistry*, 1964, **26**, 925-930.
46. R. W. M. D'Eye and G. W. Booth, *Journal of Inorganic and Nuclear Chemistry*, 1955, **1**, 326-333.
47. M. A. DeVore, C. A. Klug, M. R. Kriz, L. E. Roy and M. S. Wellons, *The Journal of Physical Chemistry A*, 2018, **122**, 6873-6878.
48. J. Yeon, M. D. Smith, A. S. Sefat, T. T. Tran, P. S. Halasyamani and H.-C. zur Loye, *Inorganic Chemistry*, 2013, **52**, 8303-8305.
49. F. Pointurier, C. Lelong and O. Marie, *Vibrational Spectroscopy*, 2020, **110**, 103145.
50. G. M. B. Zadneprovskii, S.V., *Zhurnal Struknumoi Khimii*, 1971, **12**, 831-839.